

Morphology-Controlled Reststrahlen Band and Infrared Plasmon Polariton in GaN Nanostructures

Krishna Chand Maurya,^{||} Abhijit Chatterjee,^{||} Sonnada Math Shivaprasad, and Bivas Saha*



Cite This: <https://doi.org/10.1021/acs.nanolett.2c03748>



Read Online

ACCESS |



Metrics & More



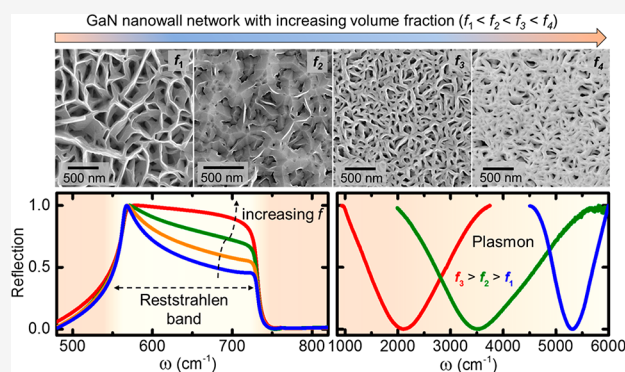
Article Recommendations



Supporting Information

ABSTRACT: Due to ultrabright and stable blue light emission, GaN has emerged as one of the most famous semiconductors of the modern era, useful for light-emitting diodes, power electronics, and optoelectronic applications. Extending GaN's optical resonance from visible to mid- and far-infrared spectral ranges will enable novel applications in many emerging technologies. Here we show hexagonal honeycomb-shaped GaN nanowall networks and vertically standing nanorods exhibiting morphology-dependent Reststrahlen band and plasmon polaritons that could be harnessed for infrared nanophotonics. Surface-induced dipoles at the edges and asperities in molecular beam epitaxy-deposited nanostructures lead to phonon absorption inside the Reststrahlen band, altering its shape from rectangular to right-trapezoidal. Excitation of such surface polariton modes provides a novel pathway to achieve far-infrared optical resonance in GaN. Additionally, surface defects in nanostructures lead to high carrier concentrations, resulting in tunable mid-infrared plasmon polaritons with high-quality factors. Demonstration of morphology-controlled Reststrahlen band and plasmon polaritons make GaN nanostructures attractive for infrared nanophotonics.

KEYWORDS: Surface Polaritons, Reststrahlen band, Plasmon polariton, GaN Nanostructure, Molecular-Beam Epitaxy, Infrared Nanophotonics



Ever since the demonstration of blue light emission in light-emitting diodes (LEDs),¹ gallium nitride (GaN) has emerged as one of the most dominating semiconducting materials over the last three decades. Numerous device technologies, such as laser diodes, transistors, high-power electronics, and optoelectronic devices based on GaN, are already commercialized.² At the same time, GaN is also actively researched for high electron mobility transistors (HEMTs), dilute magnetic semiconductors, solar cells, biosensors, photochemical water splitting, and space-related applications.^{3–5} Most of these technological advances in GaN stem from its excellent material properties, including large direct bandgap, high carrier mobility, high breakdown voltage, ease in bandgap tunability, and superior structural and chemical stability at ambient and high temperatures. However, due to the refractive index mismatch between GaN and air, the light extraction efficiency of planar GaN-based LEDs is relatively low. Similarly, planar thin-film geometry is also not ideally suited for applications such as photochemical reaction, biosensing, and others, where access to a large surface area of GaN is required.^{4,5}

To circumvent these challenges, porous hexagonal honeycomb-shaped GaN nanowall networks (NwNs) are developed that exhibit monochromatic and coherent luminescence from nanocavities, improved photocollection efficiency, and lower

dislocation densities.⁶ These nanostructures (nanorods, nanocolumns, and NwNs) exhibit sharp band-edge photoemission and almost no defect-related emission peaks often found in GaN films.⁶ By altering the growth conditions such as the substrate temperature and nitrogen and gallium flux, single-crystalline polygonal-shaped cavities with steep-wedge-shaped nanowalls with different GaN fill fractions are also developed. Cross-sectional microscopy imaging revealed that the nanowall networks are ~100–200 nm wide at the bottom, ~5–10 nm wide at the top, and exhibit micron-sized heights that can be tuned with growth durations. Significant changes in the growth parameters also result in vertically aligned nanorods that are 100–200 nm in diameter, ~1 μm in height, and are directly deposited on Si or Al₂O₃ substrates.^{7–9}

Though the visible-wavelength photoemission properties of such GaN nanostructures have been studied before, the impact of nanostructuring on GaN's infrared (IR) optical properties is

Received: September 24, 2022

Revised: November 30, 2022

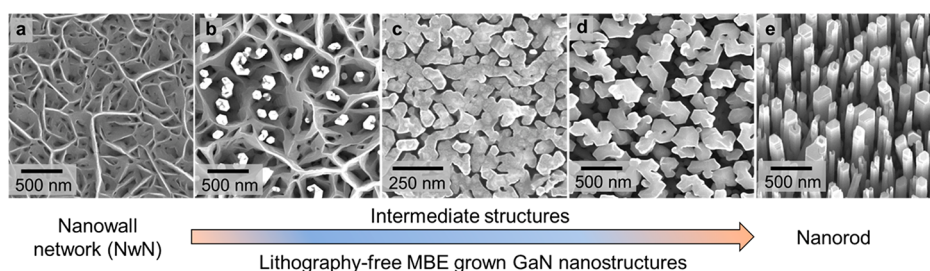


Figure 1. Plan-view FESEM microstructure of MBE-deposited GaN nanostructures. (a–e) Surface topography of nanowall network to nanorod along with various intermediate complex structures. Crystal growth under nonequilibrium conditions gives rise to such complex surface morphology.

not elucidated. Achieving optical resonances in the mid-^{10–13} and far-^{14–16} IR spectral range is necessary to further the progress in GaN research and for its potential applications^{17–20} in many emerging device technologies such as radiative cooling,²¹ solar thermophotovoltaics,^{22,23} nanolaser,²⁴ sensing,²⁵ surveillance,²⁶ etc. In general, IR light in the mid- to long-wavelength spectral range couples directly to the transverse optical (TO) phonon mode in polar semiconductors and leads to a highly reflecting region bounded by the TO and longitudinal optical (LO) phonon modes, known as the Reststrahlen band.²⁷ Inside the Reststrahlen band, the dielectric permittivity becomes negative, and the material repels the incident electric field.²⁸ The Reststrahlen effect is traditionally used to study semiconductors' vibrational properties and has also found applications in geophysics and meteorology.²⁹

For GaN epilayers deposited with molecular beam epitaxy (MBE) or metal–organic chemical vapor deposition (MOCVD), the rectangular-shaped Reststrahlen band covering a spectral range from ~ 533 to 744 cm^{-1} has been demonstrated.^{30,31} Surface phonon-polariton (SPhP) excitations are also shown in GaN thin films at $\sim 693\text{ cm}^{-1}$ within the Reststrahlen band using p-polarized light in the attenuated total reflection (ATR) measurement method.^{32,33} However, in GaN nanostructures, free surfaces, pores, and cavities are expected to impact the Reststrahlen band and alter the infrared light–matter coupling. In general, such free surfaces, edges, and asperities in the cavity lead to induced dipoles that can absorb incident light.^{34,35} Such dipole maxima appear inside the Reststrahlen band depending on the shape of the asperities and are known as the surface polaritons. Such dipolar and multipolar resonances accompany phonon absorption and can drastically impact the optical properties of materials.

In addition to the Reststrahlen effect in the far-IR spectral range, the nanostructures could also be explored as hosts for mid-IR plasmon-polariton resonance. As-deposited GaN thin films in MBE or MOCVD techniques generally possess n-type carriers due to nitrogen vacancies and oxygen as impurities. However, in GaN nanostructures, the carrier concentration is significantly higher and ranges from 10^{19} to 10^{20} cm^{-3} due to additional carrier generation from the surface vacancies and defects.⁷ Previously, density-functional theory (DFT)-based calculations have revealed that the formation energy of the nitrogen vacancy at the surface of the GaN nanostructures is more favorable than inside the bulk or inside the thin films.³⁶ Therefore, by controlling the morphology of the GaN nanostructures, their carrier concentration can be tuned, and high-quality plasmon resonance can be achieved.

In this work, we show that surface polariton excitations at the edges and asperities in GaN nanostructure significantly alter the shape of its far-IR Reststrahlen band. Located close to the LO phonon frequencies, the induced dipoles absorb optical phonons reducing the reflectance and modifying the Reststrahlen band. In addition, surface defects lead to carriers' generation, resulting in tunable plasmon resonances in the nanostructures. Excitation of the surface polaritons in the far-IR and generation of high-quality low-loss plasmon polaritons in mid-IR make GaN an attractive IR nanophotonic material.

GaN nanostructures are deposited using plasma-assisted molecular beam epitaxy (PAMBE) in an ultrahigh vacuum chamber at a base pressure of 3×10^{-11} Torr on (0001) Al_2O_3 substrates. A radio frequency (RF) plasma source operating at a forward power of 375 W was used as the nitrogen plasma source (see Supporting Information for details). The substrate temperature was maintained at $630\text{ }^\circ\text{C}$. With changes in the nitrogen and gallium flux, GaN nanowall networks with various volume fractions are obtained (see Supporting Information section-1 for details). In general, a high N_2/Ga flux ratio gives more open surfaces or a low volume fraction of GaN structure. Major changes in the growth conditions in terms of nitrogen-to-gallium flux ratio are utilized to deposit vertically aligned nanorods on Si substrates (see Supporting Information for details). For an epitaxial thin film with a smooth surface as a reference, $3\text{ }\mu\text{m}$ thick n-type GaN deposited on (0001) Al_2O_3 substrates are procured that exhibit a carrier concentration of $\sim 2 \times 10^{18}\text{ cm}^{-3}$ at room temperature.

Plan-view field-emission scanning electron microscopy (FESEM) images of GaN nanostructures (see Figure 1a–e) show the evolution of surface morphology with changes in deposition conditions. At a high substrate temperature, increased Ga adatom diffusion results in large domains of GaN that are formed both in the lateral and vertical directions (see Figure S2 in the Supporting Information). However, with the reduction of substrate temperature, the Ga adatom mobility reduces substantially, and the growth is dominated by the Volmer–Weber growth mechanism, where nitrogen-rich (N-rich) condition results in the formation of tetrahedral islands. First-principles calculations show that the adatom attachment at the edges of the tetrahedral islands is energetically favorable, which leads to an anisotropic growth resulting in the formation of “Y”-shaped structures.³⁷ With time, these structures merge and give rise to the particular NwN morphology. A further reduction in the lateral diffusion of adatoms finally leads to a nanorod morphology, as shown in Figure 1e. Such a nonequilibrium growth mode³⁸ of GaN in the MBE deposition method gives rise to complex surface

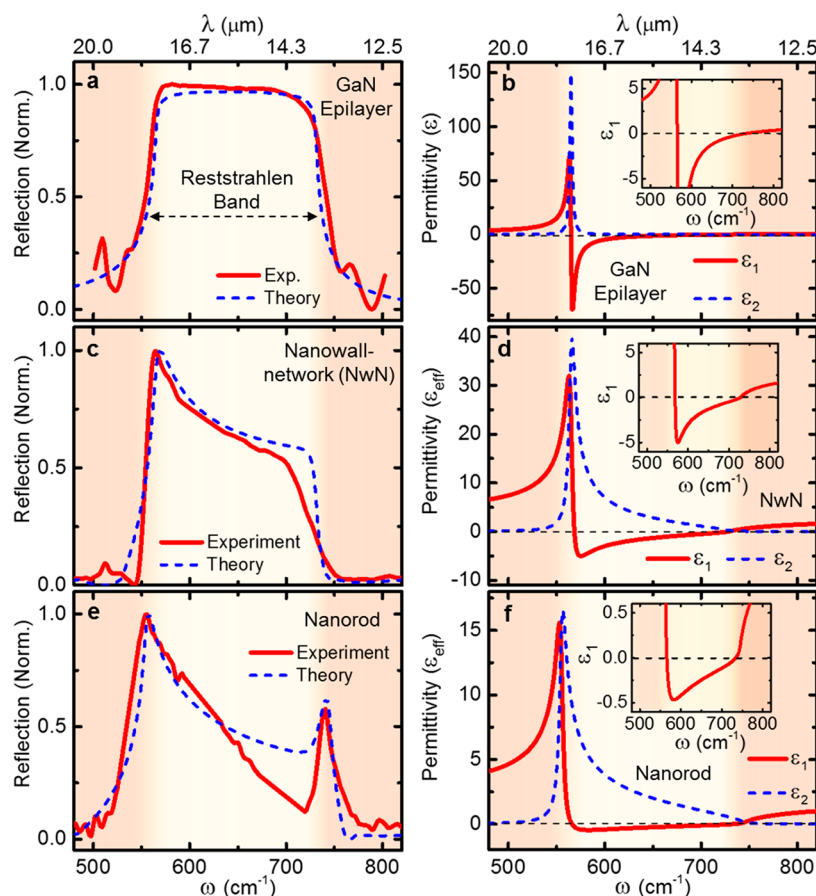


Figure 2. Reststrahlen band of GaN epilayer and nanostructures. Reflection spectrum (red curve) along with the theoretically fitted curve (blue curve) of (a) GaN epilayer, (c) GaN NwN (volume fractions of $\sim 70\%$), and (e) GaN nanorod (volume fractions of $\sim 55\%$). A highly asymmetrical right-trapezoidal-shaped Reststrahlen band appears in the GaN nanostructure. The calculated real (ϵ_1) and imaginary (ϵ_2) component of the effective dielectric permittivity (ϵ_{eff}) of (b) GaN epilayer, (d) GaN nanowall network, and (f) GaN nanorod. Nanostructuring leads to asymmetry in ENP resonance at the TO phonon frequency. To capture the sharp dip in the reflection spectrum of the nanorod near LO phonon, a phonon confinement effect^{41,42} is included in the modeling as presented in Supporting Information section 8.

patterns and nanostructures (see refs 6, 37, and 39 for a detailed discussion).

Optical characterization reveals that, compared to the rectangular-shaped Reststrahlen band in GaN epitaxial layer with a smooth surface (see Figure 2a), GaN NwN exhibits a right-trapezoid-shaped Reststrahlen band (see Figure 2c). Reflectivity in NwN decreases progressively from GaN's TO phonon frequency at 566 cm^{-1} to LO phonon frequency at 731 cm^{-1} . The optical phonon frequencies of the thin film and nanostructures are measured using Raman spectroscopy and presented in Supporting Information section 4. To obtain the dielectric permittivity, the measured reflection spectrum is fitted with Fresnel's equation. The frequency-dependent total dielectric permittivity ($\epsilon_{\text{total}}(\omega)$) is expressed as follows.⁴⁰

$$\begin{aligned}\epsilon_{\text{total}}(\omega) &= \epsilon_1 + i\epsilon_2 \\ &= \epsilon_{\infty} \left(1 - \frac{\omega_p^2}{\omega^2 - i\gamma\omega} + \frac{\omega_{\text{LO}}^2 - \omega_{\text{TO}}^2}{\omega_{\text{TO}}^2 - \omega^2 - i\omega\Gamma} \right)\end{aligned}\quad (1)$$

$$\omega_p = \sqrt{\frac{ne^2}{m^*\epsilon_0}}\quad (2)$$

$$\epsilon_{\text{plasmon}}(\omega) = -\frac{\omega_p^2}{\omega^2 - i\gamma\omega}\quad (3)$$

Here the second term corresponds to the plasmon or Drude component, while the third term refers to the phonon resonance. ω_{LO} (ω_{TO}) are the LO (TO) phonon frequencies, Γ is the phonon damping constant for phonon scattering, ϵ_{∞} is the background permittivity due to bound charges (5.35), and ω_p , γ , n , and m^* are the high-frequency dielectric constant, plasma frequency, plasmon damping constants, carrier concentration and effective mass, respectively. Since the GaN epitaxial layer exhibits a very low carrier concentration ($\sim 2 \times 10^{18}\text{ cm}^{-3}$), the electronic contribution to the dielectric permittivity in the mid- to long-wavelength IR spectral range can be neglected. However, for the NwN, since the carrier concentration is relatively large (in the $\sim 10^{19}$ – 10^{20} cm^{-3} range), an electronic contribution to the permittivity is included in modeling the Reststrahlen band spectral region.

The calculated real part of the dielectric permittivity (ϵ_1) for the epitaxial layer undergoes a positive-to-negative transition at the LO phonon mode frequency (see Figure 2b). The ϵ_1 remains negative within the Reststrahlen band and exhibits an epsilon-near-pole (ENP) resonance at the TO phonon frequency. As light couples directly to the TO phonon mode, the imaginary part of the dielectric permittivity,

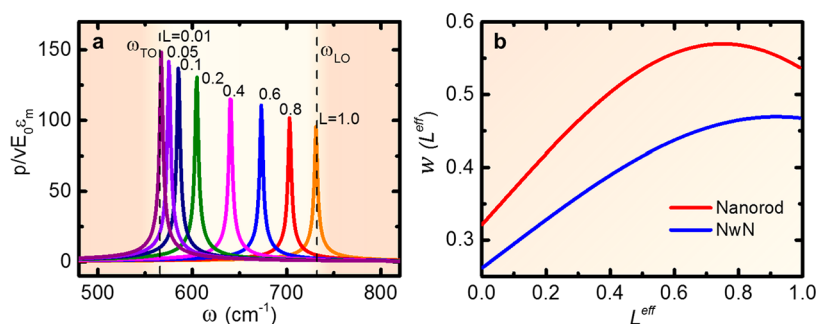


Figure 3. Induced dipole moment and its distribution within the Reststrahlen band. (a) Normalized induced dipole moments of the surface polaritons as a function of wavenumber with depolarization factor L as a parameter. For L close to 1, the surface polariton maximum appears close to the LO phonon frequency, while for L close to zero, surface polariton maxima are located close to the TO phonon frequency. (b) The probability distribution function for dipole absorption as a function of effective depolarization factor of GaN nanostructure.

represented as the optical loss, exhibits a sharp symmetric peak located at TO phonon frequency, as shown in Figure 2b.

Since the NwN and nanorods contain voids and asperities, effectively reducing the GaN fill fraction, the infrared reflection spectrum of the nanostructures is modeled using Fresnel's equation with Lichtenecker's effective medium approximation (LEMA).⁴³ The expression for the effective permittivity ($\epsilon_{\text{eff}} = \epsilon_1 + i\epsilon_2$) can be presented as

$$\log \epsilon_{\text{eff}} = f \log \epsilon_i + (1 - f) \log \epsilon_s \quad (4)$$

where f is the volume fraction of GaN, and $\epsilon_i(\epsilon_s)$ is the permittivity of the GaN (air). LEMA softens the dielectric constant of GaN with its fill fraction f .

Compared to the epitaxial layer, the dielectric permittivity of NwN exhibits (see Figure 2d) an asymmetric response due to the asymmetry in the reflection spectrum (see Figure 2c). Starting from the ENP resonance at the TO phonon frequency, the real component of the effective dielectric permittivity ($\text{Re}[\epsilon_{\text{eff}}]$ or ϵ_1) is smeared toward the LO phonon frequency (see Figure 2d). Similarly, the optical loss ($\text{Im}[\epsilon_{\text{eff}}]$ or ϵ_2) also shows an asymmetric peak at the ENP. Optical losses are also found away from the TO phonon frequency due to the phonon absorptions. The magnitude of $\text{Re}[\epsilon_{\text{eff}}]$ in NwN is also smaller than that of the $\text{Re}[\epsilon]$ of GaN epitaxial layers due to the decrease in the effective volume fraction of GaN inside the NwN.

Compared to the NwN, the reflection spectrum of the nanorod structure exhibits a much more significant asymmetry (see Figure 2e), with a pronounced dip at $\sim 720 \text{ cm}^{-1}$. Reflectivity recovers slightly at the position of the LO phonon frequency before vanishing outside of the Reststrahlen band spectral region, thus exhibiting a peak-like feature. Extraction of the dielectric permittivity shows higher asymmetry in the real component of the dielectric permittivity with very small values of $\text{Re}[\epsilon_{\text{eff}}]$ or ϵ_1 and minimal dispersion as the LO phonon frequency is approached (see Figure 2f). The values of $\text{Re}[\epsilon_{\text{eff}}]$ or ϵ_1 are also much smaller compared to the ones determined for the NwN. Notably, while the optical loss is nearly negligible in the region close to the LO phonon frequency in an epitaxial film, $\text{Im}[\epsilon_{\text{eff}}]$ or ϵ_2 of the nanorod is significant in the regions close to the LO phonon frequency, highlighting a great extent of optical absorption away from the TO phonon frequency region.

The origin of the changes in the shape of the Reststrahlen band can be explained due to the dipole-induced phonon absorption at the surfaces, edges, and asperities in the

nanostructures. The distribution of the size and shape of the asperities ensures multiple dipole peaks with various degrees of geometrical factors (or depolarization factor), which essentially results in a tapered decrease in the reflectivity from the TO frequency to LO frequency. Following the description of previous work,³⁴ the generation of the surface polariton is modeled by assuming the asperities as having ellipsoidal shapes with dimensions much smaller compared to the wavelength of light. The induced dipole moment (p) in the ellipsoid is calculated by eq 5³⁵

$$p = v \frac{\epsilon - \epsilon_m}{\epsilon_m + L_j(\epsilon - \epsilon_m)} \epsilon_m E_0 \quad (5)$$

where v is the volume of the ellipsoidal particle ($4\pi abc/3$); a , b , and c are the principal semi-axes of the ellipsoid. ϵ and ϵ_m are the dielectric permittivity of GaN and the matrix (air), respectively. E_0 is the electric field of the light. Here L_j is the geometrical factor along the j th principal axis of the ellipsoid with $L_1 + L_2 + L_3 = 1$. The geometrical factor depends on the shape of the structure.

Figure 3a shows that the induced dipole maxima (or surface polariton) appearing closer to the LO phonon frequency exhibit high depolarization factors (L close to 1). On the other hand, for L approaching zero, the induced dipole modes appear close to TO phonon frequency. However, since the dipoles interact with those from the surface and with each other, and due to the fact that the asperities are not perfectly ellipsoidal, several induced dipoles with different depolarization factors can arise inside the Reststrahlen band. To determine the dominating L values for the GaN nanostructures, Andersson and Ribbing formalism³⁴ is utilized (see eq 6), which correlates the induced dipole probability with the effective geometrical factor (L^{eff}) and effective permittivity ($\epsilon_{\text{eff}}^{\text{phonon}}$) of the complex structures.

$$\epsilon_{\text{eff}}^{\text{phonon}} = \epsilon + f(\epsilon - \epsilon_m) \epsilon_m \int_0^1 \frac{w(L^{\text{eff}})}{\epsilon_m + L^{\text{eff}}(\epsilon - \epsilon_m)} dL^{\text{eff}} \quad (6)$$

Here, $w(L^{\text{eff}})$ is the probability function for an induced dipole, which depends on the effective depolarization factor L^{eff} or the topography of the surfaces (see Supporting Information section 6).⁴⁴ In general, for planar flat flakes, the probability function exhibits a large contribution for L^{eff} less than 1/3 (see Supporting Information sections 5 and 6 for details). In the case of round edges or spherical surfaces, the probability function exhibits maxima for $L^{\text{eff}} = 1/3$, while for out-of-plane

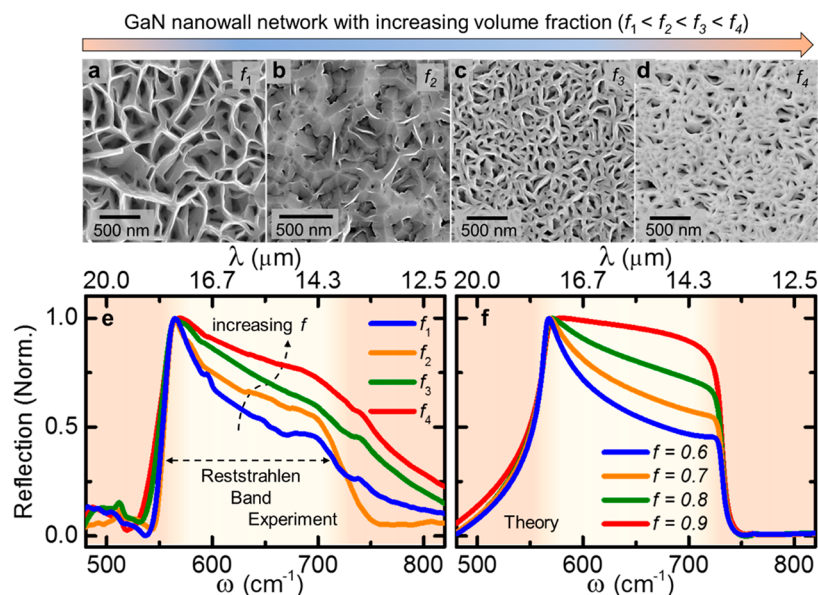


Figure 4. Impact of GaN volume fraction on nanostructure's Reststrahlen band. FESEM images of GaN NwNs with increasing volume fraction (a) f_1 (~ 0.60), (b) f_2 (~ 0.70), (c) f_3 (~ 0.77), and (d) f_4 (~ 0.83). (e) Experimentally measured reflection curve of the NwNs. (f) Calculated reflection curve using LEMA for volume fraction of 0.6, 0.7, 0.8, or 0.9. Both the experimental and the theoretical results show that a lower volume fraction of GaN leads to higher asymmetry in the Reststrahlen band.

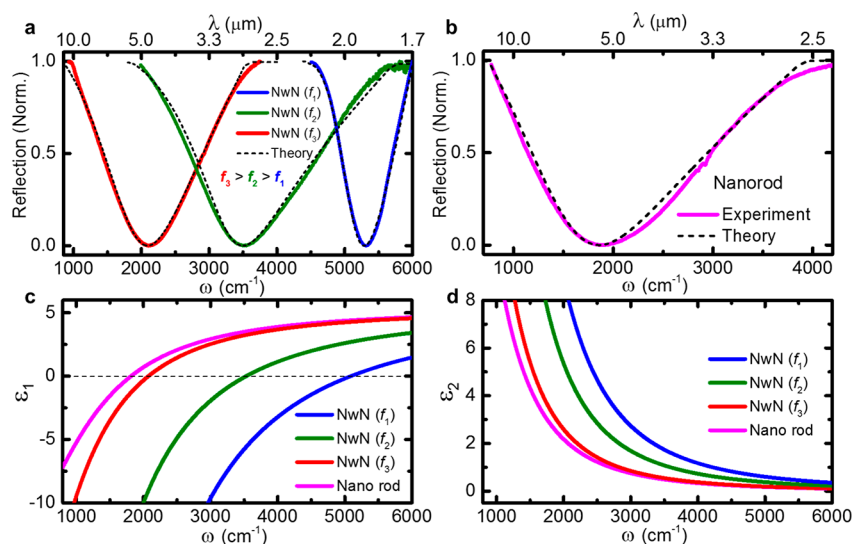


Figure 5. Plasmon polariton in GaN nanostructures. (a) Plasmon response in GaN NwNs with volume fraction f_1 (blue curve), f_2 (green curve), and f_3 (red curve), where $f_3 > f_2 > f_1$. (b) Plasmon response in GaN nanorods. GaN NwNs exhibit more open surfaces compared to nanorods; consequently, more carriers are present in NwNs. The (c) real (ϵ_1) and (d) imaginary (ϵ_2) component of the dielectric permittivity of GaN NwNs of volume fraction f_1 (blue curve), f_2 (green curve), f_3 (red curve), and nanorod (magenta curve).

(vertically standing) sharp asperities, the probability function contributes more near regions where the L^{eff} values are close to 1. In the case of the GaN NwN and nanorods, the probability function contributes more to the higher values of L^{eff} as the nanostructures exhibit needle-like asperities. Figure 3b shows that $w(L^{\text{eff}})$ increases monotonically with L^{eff} for the NwN, which explains the continuous decrease in the reflectivity of GaN NwN from TO-to-LO mode. On the other hand, $w(L^{\text{eff}})$ exhibits a maximum for the L^{eff} between 0.6 and 0.85 for the nanorod that leads to a dip in reflection inside the Reststrahlen band (see Figure 2e). The magnitude of $w(L^{\text{eff}})$ for the nanorods is also higher than the NwN, which explains the higher absorption in the nanorods.

To determine the effects of fill fraction on NwN's optical properties, Reststrahlen bands are measured with varying f , ranging from $\sim 60\%$ to $\sim 83\%$. With a decrease in f , the Reststrahlen bands appear more asymmetric (see Figure 4e), and reflection decreases progressively as one moves away from the TO phonon to LO phonon frequency. As the FESEM images show (see Figure 4a–d), GaN NwN with a lower volume fraction (f_1) has more open surfaces and edges than the NwN with a high-volume fraction (f_4). Consequently, more surface polariton absorption takes place in NwN (f_1) resulting in more asymmetry in the Reststrahlen band. This phenomenon is further verified by calculating the dielectric permittivity using the LEMA and by determining the theoretical reflection curve, where the volume fraction (f) is

Table 1. Plasmonic and Electrical Properties of the GaN Nanostructures

GaN nanostructures	resonance energy (E_p) (cm^{-1})	fwhm (ΔE) (meV)	carrier concentration (cm^{-3})	mobility ($\text{cm}^2/(\text{V s})$)	optical loss (ϵ_2) at E_p
NwN (f_1)	5316	200	3.2×10^{20}	29	0.5
NwN (f_2)	3530	240	1.7×10^{20}	12	1.6
NwN (f_3)	2116	193	6.1×10^{19}	15	2.1
NwN (f_4)	1911	152	4.7×10^{19}	19	1.9
nanorod	1892	220	4.5×10^{19}	13	2.2

decreased from 0.9 to 0.6. A clear decrease in reflectivity can be found in Figure 4f, which leads to a more right-trapezoidal-shaped Reststrahlen band with a reduction in GaN volume fraction. Apart from the decrease in the ϵ_1 of the nanostructure with decreasing GaN fill fraction, larger asymmetry is found on both ϵ_1 and ϵ_2 with respect to the ENP at the TO phonon frequency (see Figure S8).

Apart from the changes in the shape of the Reststrahlen band, our results also show that nanostructuring alters far-IR optical properties of GaN, such as thermal emission. The emission spectra are measured by mounting the samples on a copper hot plate, from where the radiation is collected in the Fourier transform infrared (FTIR) spectrometer (see Figure S10). Thermal emission of the NwN follows the inverse of the asymmetric Reststrahlen band of the nanostructure (see Supporting Information section-9 for details). Since, according to Kirchhoff's law, emissivity is same as the absorptivity, the measured emission spectrum is expected to follow the opposite trend of the Reststrahlen band.

Along with the influence on the Reststrahlen band, nanostructuring in GaN also produces plasmon resonance in the mid-IR spectral range. Since the nitrogen vacancies are easier to form on the free surfaces, exposed surfaces of the GaN structures lead to a higher concentration of nitrogen vacancies resulting in a large carrier concentration. Reflectivity measurements in the mid-IR spectral range show that, for NwNs, the plasmon resonance appears at 5316 cm^{-1} ($1.86 \mu\text{m}$), 3532 cm^{-1} ($2.83 \mu\text{m}$), 2116 cm^{-1} ($4.72 \mu\text{m}$), and 1911 cm^{-1} ($5.23 \mu\text{m}$) for volume fractions f_1 , f_2 , f_3 , and f_4 , respectively (see Figure 5a,b, reflection of GaN (f_4) is shown in Supporting Information Figure S11). The lowest volume fraction GaN (f_1) NwN has the highest exposed free surface as well as the highest free carriers (see Table 1). In the case of GaN nanorod, a minimum in the reflection spectrum at 1892 cm^{-1} ($5.28 \mu\text{m}$) is obtained that corresponds to the free-carrier plasmon resonances. Utilizing the Drude function (eq 3), reflection spectra are modeled using Fresnel's equation, and the dielectric permittivity is obtained.

The ϵ_1 of NwN (f_1) to NwN (f_4) and nanorod exhibit a positive-to-negative crossover at 5113, 3515, 2065, 1820, and 1808 cm^{-1} , respectively, near to their plasma frequency, also known as the epsilon-near-zero (ENZ) frequency (see Figure 5c). Note that plasma frequency and ENZ frequency coincide with each other only in the case of a lossless medium. In the present samples, GaN NwN (f_1) has the lowest optical loss (ϵ_2) at the plasmon resonance frequency (see Figure 5d), which is lower than the ϵ_2 of visible plasmonic materials such as Au,⁴⁵ refractory transition metals,⁴⁶ metal nitrides TiN^{11,12} and IR plasmonic materials such as ScN,^{16,47} transparent conducting oxides,¹² etc.

A comparison of the plasma frequency, damping factor, and the plasmon resonance quality factor of GaN NwNs with other well-established IR plasmonic materials show (see Figure S12) that, depending on the fill fraction, the NwNs and nanorods

exhibit plasma frequencies that span a significant spectral range. The quality factor of the NwN's plasma resonance is also comparable to, or higher than, other mid-infrared plasmonic nanostructures such as InN,⁴⁸ Al/ZnO,⁴⁹ Cu_{2-x}S ,⁵⁰ $\text{Sn/In}_2\text{O}_3$,⁵¹ and $\text{Ce/In}_2\text{O}_3$ ⁵² due to its low optical losses.

In conclusion, optical resonance in GaN is extended from visible to far- and mid-infrared spectral regions by the excitation of surface-polariton and plasmon polariton modes in nanostructures, respectively. Single-crystalline hexagonal honeycomb-shaped GaN nanowall network and vertically standing nanorods are developed with a plasma-assisted molecular beam epitaxy (PAMBE). Surface polaritons resulting from the dipole-induced phonon absorption at surfaces, edges, and asperities in nanostructures are found to control the shape of the Reststrahlen band. Most surface polaritons occur close to the LO mode frequency due to the geometry of the sharp needle-like asperities standing out of the surface. The Reststrahlen band shape changed to right-trapezoidal with increased asperities and pore volume fraction from a rectangular shape in the planar epitaxial thin film. Free surfaces of the nanostructure also generate carriers with high concentrations, resulting in mid-infrared plasmon resonance with high-quality factors. Demonstration of morphology-controlled infrared resonances in GaN will further its progress in thermophotovoltaics, IR sensors, emitters, and other emerging device technologies.

■ ASSOCIATED CONTENT

Data Availability Statement

The data that supports the findings of this study are available from the corresponding author upon reasonable request.

Supporting Information

The Supporting Information is available free of charge at <https://pubs.acs.org/doi/10.1021/acs.nanolett.2c03748>.

Details of sample preparation, optical measurements (Raman and Fourier-transform infrared spectroscopy), and detailed analysis of results (PDF)

■ AUTHOR INFORMATION

Corresponding Author

Bivas Saha – Chemistry and Physics of Materials Unit, International Centre for Materials Science, and School of Advanced Materials, Jawaharlal Nehru Centre for Advanced Scientific Research, Bangalore 560064, India; orcid.org/0000-0002-0837-1506; Email: bsaha@jncasr.ac.in, bivas.mat@gmail.com

Authors

Krishna Chand Maurya – Chemistry and Physics of Materials Unit, International Centre for Materials Science, and School of Advanced Materials, Jawaharlal Nehru Centre for Advanced Scientific Research, Bangalore 560064, India

Abhijit Chatterjee – Chemistry and Physics of Materials Unit, International Centre for Materials Science, and School of Advanced Materials, Jawaharlal Nehru Centre for Advanced Scientific Research, Bangalore 560064, India

Sonnada Math Shivaprasad – Chemistry and Physics of Materials Unit, International Centre for Materials Science, and School of Advanced Materials, Jawaharlal Nehru Centre for Advanced Scientific Research, Bangalore 560064, India

Complete contact information is available at:

<https://pubs.acs.org/10.1021/acs.nanolett.2c03748>

Author Contributions

[†]These authors contributed equally to this work.

Notes

The authors declare no competing financial interest.

ACKNOWLEDGMENTS

K.C.M. and B.S. acknowledge International Centre for Materials Science and Sheikh Saqr Laboratory in JNCASR for support. B.S. acknowledges the Young Scientist Research Award from the Board of Research in Nuclear Sciences (BRNS), Department of Atomic Energy, India, with Grant No. 59/20/10/2020-BRNS/59020 for financial support. K.C.M. thanks Council of Scientific & Industrial Research for fellowship.

REFERENCES

- (1) Nakamura, S.; Krames, M. R. History of Gallium-Nitride-Based Light-Emitting Diodes for Illumination. *Proc. IEEE* **2013**, *101* (10), 2211–2220.
- (2) Pearton, S. J.; Abernathy, C. R.; Overberg, M. E.; Thaler, G. T.; Onstine, A. H.; Gila, B. P.; Ren, F.; Lou, B.; Kim, J. New Applications for Gallium Nitride. *Mater. Today* **2002**, *5* (6), 24–31.
- (3) Liu, C.; Yun, F.; Morkoç, H. Ferromagnetism of ZnO and GaN: A Review. *J. Mater. Sci. Mater. Electron.* **2005**, *16* (9), 555–597.
- (4) Xiao, Y.; Vanka, S.; Pham, T. A.; Dong, W. J.; Sun, Y.; Liu, X.; Navid, I. A.; Varley, J. B.; Hajibabaei, H.; Hamann, T. W.; Ogitsu, T.; Mi, Z. Crystallographic Effects of GaN Nanostructures in Photoelectrochemical Reaction. *Nano Lett.* **2022**, *22* (6), 2236–2243.
- (5) Han, S.; Noh, S.; Yu, Y. T.; Lee, C. R.; Lee, S. K.; Kim, J. S. Highly Efficient Photoelectrochemical Water Splitting Using GaN-Nanowire Photoanode with Tungsten Sulfides. *ACS Appl. Mater. Interfaces* **2020**, *12* (52), 58028–58037.
- (6) Chatterjee, A.; Acharya, S.; Shivaprasad, S. M. Morphology-Related Functionality in Nanoarchitected GaN. *Annu. Rev. Mater. Res.* **2020**, *50* (July), 179–206.
- (7) Zhong, A.; Fan, P.; Zhong, Y.; Zhang, D.; Li, F.; Luo, J.; Xie, Y.; Hane, K. Structure Shift of GaN Among Nanowall Network, Nanocolumn, and Compact Film Grown on Si (111) by MBE. *Nanoscale Res. Lett.* **2018**, *13*, 1–7.
- (8) Consonni, V. Self-Induced Growth of GaN Nanowires by Molecular Beam Epitaxy: A Critical Review of the Formation Mechanisms. *Phys. Status Solidi - Rapid Res. Lett.* **2013**, *7* (10), 699–712.
- (9) Avit, G.; Lekhal, K.; André, Y.; Bougerol, C.; Réveret, F.; Leymarie, J.; Gil, E.; Monier, G.; Castelluci, D.; Trassoudaine, A. Ultralong and Defect-Free GaN Nanowires Grown by the HVPE Process. *Nano Lett.* **2014**, *14* (2), 559–562.
- (10) Metaxa, C.; Kassavetis, S.; Pierson, J. F.; Gall, D.; Patsalas, P. Infrared Plasmonics with Conductive Ternary Nitrides. *ACS Appl. Mater. Interfaces* **2017**, *9* (12), 10825–10834.
- (11) Maurya, K. C.; Shalaev, V. M.; Boltasseva, A.; Saha, B. Reduced Optical Losses in Refractory Plasmonic Titanium Nitride Thin Films Deposited with Molecular Beam Epitaxy. *Opt. Mater. Express* **2020**, *10* (10), 2679.
- (12) Naik, G. V.; Shalaev, V. M.; Boltasseva, A. Alternative Plasmonic Materials: Beyond Gold and Silver. *Adv. Mater.* **2013**, *25* (24), 3264–3294.
- (13) Runnerstrom, E. L.; Kelley, K. P.; Sachet, E.; Shelton, C. T.; Maria, J. P. Epsilon-near-Zero Modes and Surface Plasmon Resonance in Fluorine-Doped Cadmium Oxide Thin Films. *ACS Photonics* **2017**, *4* (8), 1885–1892.
- (14) Foteinopoulou, S.; Devarapu, G. C. R.; Subramania, G. S.; Krishna, S.; Wasserman, D. Phonon-Polaritonics: Enabling Powerful Capabilities for Infrared Photonics. *Nanophotonics* **2019**, *8* (12), 2129–2175.
- (15) Caldwell, J. D.; Glembocki, O. J.; Francescato, Y.; Sharac, N.; Giannini, V.; Bezares, F. J.; Long, J. P.; Owrutsky, J. C.; Vurgaftman, I.; Tischler, J. G.; Wheeler, V. D.; Bassim, N. D.; Shirey, L. M.; Kasica, R.; Maier, S. A. Low-Loss, Extreme Subdiffraction Photon Confinement via Silicon Carbide Localized Surface Phonon Polariton Resonators. *Nano Lett.* **2013**, *13* (8), 3690–3697.
- (16) Maurya, K. C.; Rao, D.; Acharya, S.; Rao, P.; Pillai, A. I. K.; Selvaraja, S. K.; Garbrecht, M.; Saha, B. Polar Semiconducting Scandium Nitride as an Infrared Plasmon and Phonon–Polaritonic Material. *Nano Lett.* **2022**, *22* (13), 5182–5190.
- (17) Caldwell, J. D.; Vurgaftman, I.; Tischler, J. G.; Glembocki, O. J.; Owrutsky, J. C.; Reinecke, T. L. Atomic-Scale Photonic Hybrids for Mid-Infrared and Terahertz Nanophotonics. *Nat. Nanotechnol.* **2016**, *11* (1), 9–15.
- (18) Sanvitto, D.; Kéna-Cohen, S. The Road towards Polaritonic Devices. *Nat. Mater.* **2016**, *15* (10), 1061–1073.
- (19) Kinsey, N.; DeVault, C.; Boltasseva, A.; Shalaev, V. M. Near-Zero-Index Materials for Photonics. *Nat. Rev. Mater.* **2019**, *4*, 742–760.
- (20) Jahani, S.; Jacob, Z. All-Dielectric Metamaterials. *Nat. Nanotechnol.* **2016**, *11* (1), 23–36.
- (21) Hossain, M. M.; Jia, B.; Gu, M. A Metamaterial Emitter for Highly Efficient Radiative Cooling. *Adv. Opt. Mater.* **2015**, *3* (8), 1047–1051.
- (22) Chang, C. C.; Kort-Kamp, W. J. M.; Nogan, J.; Luk, T. S.; Azad, A. K.; Taylor, A. J.; Dalvit, D. A. R.; Sykora, M.; Chen, H. T. High-Temperature Refractory Metasurfaces for Solar Thermophotovoltaic Energy Harvesting. *Nano Lett.* **2018**, *18* (12), 7665–7673.
- (23) Chirumamilla, M.; Chirumamilla, A.; Yang, Y.; Roberts, A. S.; Kristensen, P. K.; Chaudhuri, K.; Boltasseva, A.; Sutherland, D. S.; Bozhevolnyi, S. I.; Pedersen, K. Large-Area Ultrabroadband Absorber for Solar Thermophotovoltaics Based on 3D Titanium Nitride Nanopillars. *Adv. Opt. Mater.* **2017**, *5* (22), 1700552.
- (24) Azzam, S. I.; Kildishev, A. V.; Ma, R. M.; Ning, C. Z.; Oulton, R.; Shalaev, V. M.; Stockman, M. I.; Xu, J. L.; Zhang, X. Ten Years of Spasers and Plasmonic Nanolasers. *Light Sci. Appl.* **2020**, *9* (1). DOI: 10.1038/s41377-020-0319-7.
- (25) Lewis, R. A. A Review of Terahertz Detectors. *J. Phys. D: Appl. Phys.* **2019**, *52* (43), 433001.
- (26) Corsi, C. Infrared: A Key Technology for Security Systems. *Adv. Opt. Technol.* **2012**, *2012* (2), 1.
- (27) Adachi, S. The Reststrahlen Region. In *Optical Properties of Crystalline and Amorphous Semiconductors*; Springer US: Boston, MA, 1999; Vol. 5, pp 33–62. DOI: 10.1007/978-1-4615-5241-3_2.
- (28) Strosio, M. A.; Dutta, M. Phonons in Bulk Würtzite Crystal. In *Phonons in Nanostructures*; Cambridge University Press, 2001; pp 16–25. DOI: 10.1017/CBO9780511534898.004.
- (29) Shirley, K. A.; Glotch, T. D. Particle Size Effects on Mid-Infrared Spectra of Lunar Analog Minerals in a Simulated Lunar Environment. *J. Geophys. Res. Planets* **2019**, *124* (4), 970–988.
- (30) Barker, A. S.; Ilegems, M. Infrared Lattice Vibrations and Free-Electron Dispersion in GaN. *Phys. Rev. B* **1973**, *7* (2), 743–750.
- (31) Azuhata, T.; Matsunaga, T.; Shimada, K.; Yoshida, K.; Sota, T.; Suzuki, K.; Nakamura, S. Optical Phonons in GaN. *Phys. B Condens. Matter* **1996**, *219–220* (1–4), 493–495.
- (32) Ng, S. S.; Hassan, Z.; Abu Hassan, H. Surface Phonon Polariton of Wurtzite GaN Thin Film Grown on C-Plane Sapphire Substrate. *Solid State Commun.* **2008**, *145* (11–12), 535–538.

- (33) Torii, K.; Koga, T.; Sota, T.; Azuhata, T.; Chichibu, S. F.; Nakamura, S. An Attenuated-Total-Reflection Study on the Surface Phonon-Polariton in GaN. *J. Phys.: Condens. Matter* **2000**, *12* (31), 7041–7044.
- (34) Andersson, S. K.; Ribbing, C. G. Light Extinction by Bulk Voids and Surface Irregularities in Ceramic Materials. *Phys. Rev. B* **1994**, *49* (16), 11336–11343.
- (35) Bohren, C. F. Particles Small Compared with the Wavelength. In *Absorption and Scattering of Light by Small Particles*; Wiley-VCH Verlag GmbH: Weinheim, Germany, 2007; pp 130–157. DOI: 10.1002/9783527618156.ch5.
- (36) Nayak, S.; Naik, M. H.; Jain, M.; Waghmare, U. V.; Shivaprasad, S. M. First-Principles Theoretical Analysis and Electron Energy Loss Spectroscopy of Vacancy Defects in Bulk and Nonpolar (10 $\bar{1}$ 0) Surface of GaN. *J. Vac. Sci. Technol. A* **2020**, *38* (6), 063205.
- (37) Nayak, S.; Kumar, R.; Shivaprasad, S. M. Edge Enhanced Growth Induced Shape Transition in the Formation of GaN Nanowall Network. *J. Appl. Phys.* **2018**, *123* (1), 014302.
- (38) Ben-Jacob, E.; Garik, P. The Formation of Patterns in Non-Equilibrium Growth. *Nature* **1990**, *343* (6258), 523–530.
- (39) Kesaria, M.; Shetty, S.; Shivaprasad, S. M. Evidence for Dislocation Induced Spontaneous Formation of GaN Nanowalls and Nanocolumns on Bare C-Plane Sapphire. *Cryst. Growth Des.* **2011**, *11* (11), 4900–4903.
- (40) Folland, T. G.; Nordin, L.; Wasserman, D.; Caldwell, J. D. Probing Polaritons in the Mid- to Far-Infrared. *J. Appl. Phys.* **2019**, *125* (19), 191102.
- (41) Arora, A. K.; Rajalakshmi, M.; Ravindran, T. R.; Sivasubramanian, V. Raman Spectroscopy of Optical Phonon Confinement in Nanostructured Materials. *J. Raman Spectrosc.* **2007**, *38* (6), 604–617.
- (42) Kushvaha, S. S.; Kumar, M. S.; Shukla, A. K.; Yadav, B. S.; Singh, D. K.; Jewariya, M.; Ragam, S. R.; Maurya, K. K. Structural, Optical and Electronic Properties of Homoepitaxial GaN Nanowalls Grown on GaN Template by Laser Molecular Beam Epitaxy. *RSC Adv.* **2015**, *5* (107), 87818–87830.
- (43) Sihvola, A. Generalised Mixing Rules. In *Electromagnetic Mixing Formulas and Applications*; Institution of Engineering and Technology, 1999; pp 161–176. DOI: 10.1049/PBEW047E_ch9.
- (44) Tazawa, M.; Fujii, A.; Tanemura, S. The Surface Substructural Effects on Reststrahlen Bands in Reflectance of Alumina Ceramics with Different Sized Grains. *Netsu Bussei* **1995**, *9* (3), 157–162.
- (45) Johnson, P. B.; Christy, R. W. Optical Constant of the Nobel Metals. *Phys. Rev. B* **1972**, *6* (12), 4370–4379.
- (46) Maurya, K. C.; Biswas, B.; Rao, D.; Saha, B. Giant Enhancement of Plasmonic Response and Epsilon-near-Zero Signature in Refractory Transition Metals (Ta, W, and Mo) Deposited at High-Temperature. *Appl. Phys. Lett.* **2021**, *118* (4), 041902.
- (47) Maurya, K. C.; Biswas, B.; Garbrecht, M.; Saha, B. Wave-Vector-Dependent Raman Scattering from Coupled Plasmon–Longitudinal Optical Phonon Modes and Fano Resonance in n-type Scandium Nitride. *Phys. Status Solidi RRL* **2019**, *13* (9), 1900196.
- (48) Askari, S.; Mariotti, D.; Stehr, J. E.; Benedikt, J.; Keraudy, J.; Helmersson, U. Low-Loss and Tunable Localized Mid-Infrared Plasmons in Nanocrystals of Highly Degenerate InN. *Nano Lett.* **2018**, *18* (9), 5681–5687.
- (49) Greenberg, B. L.; Ganguly, S.; Held, J. T.; Kramer, N. J.; Mkhoyan, K. A.; Aydil, E. S.; Kortshagen, U. R. Nonequilibrium-Plasma-Synthesized ZnO Nanocrystals with Plasmon Resonance Tunable via Al Doping and Quantum Confinement. *Nano Lett.* **2015**, *15* (12), 8162–8169.
- (50) Luther, J. M.; Jain, P. K.; Ewers, T.; Alivisatos, A. P. Localized Surface Plasmon Resonances Arising from Free Carriers in Doped Quantum Dots. *Nat. Mater.* **2011**, *10* (5), 361–366.
- (51) Lounis, S. D.; Runnerstrom, E. L.; Bergerud, A.; Nordlund, D.; Milliron, D. J. Influence of Dopant Distribution on the Plasmonic Properties of Indium Tin Oxide Nanocrystals. *J. Am. Chem. Soc.* **2014**, *136* (19), 7110–7116.
- (52) Runnerstrom, E. L.; Bergerud, A.; Agrawal, A.; Johns, R. W.; Dahlman, C. J.; Singh, A.; Selbach, S. M.; Milliron, D. J. Defect Engineering in Plasmonic Metal Oxide Nanocrystals. *Nano Lett.* **2016**, *16* (5), 3390–3398.